Desalination and Water Treatment
www.deswater.com

doi: 10.5004/dwt.2021.27099

223 (2021) 54–70
May

Optimization of hydrodynamic vortex separator for removal of sand particles from storm water by computational fluid dynamics

Mahaveer[a], Xue-yi You[a,b,*]

[a]*School of Environmental Science and Engineering, Tianjin University, Tianjin 300350, China, Tel. +86-22-27403561; emails: xyyou@tju.edu.cn (X.-Y. You), langhanimahaveer@tju.edu.cn (Mahaveer)*
[b]*Tianjin Engineering Centre of Urban River Eco-Purification Technology*

Received 7 July 2020; Accepted 29 January 2021

ABSTRACT

Storm water treatment has been gradually acknowledged for the removal of pollutants from urban areas using the hydro cyclone separation technique. The separation efficiency of the hydrodynamic vortex separator (HDVS) is a complex phenomenon. With the aim enhance the separation potency of HDVS for storm runoff to get rid of sand particles, the HDVS with different structural configurations was studied by computational fluid dynamics. A steady-state model was created to simulate the HDVS, where the simulation of solid–liquid part flow within the HDVS was conducted by 3-D Eulerian–Eulerian multiphase model and Reynolds stress model combined with the kinetic theory of granular flow. The rate contours, recess, outlet volume fraction of solid phase and particle removal efficiency were specially analyzed. The simulation results showed that the separation efficiency of HDVS had a positive relation to different structural configurations. The optimal design parameters of HDVS were obtained. The great agreement of flow rate and alter the law of separation potency proves that the mentioned multiphase is in-line accustomed to optimize the separation efficiency of hydrodynamic vortex separator.

Keywords: Computational fluid dynamics; Hydrodynamic vortex separator; Kinetic theory of granular flow; Numerical simulation; Reynolds stress model

1. Introduction

Urbanization and human development had adverse impact on the earth's hydrological cycle by increasing the area of impermeable surfaces (such as parking lots, paved roads, roofs, driveway, sidewalks, etc.), and thereby increased pollutants. Pollutants and other threats are becoming increasingly prevalent nowadays. Therefore, stormwater runoff must be treated under sticker policy before entering the receiving water system so that it can better serve our society. Numerous structural best management practices (BMPs) have been utilized to deal with these issues such as hydrodynamic vortex separators (HDVSs), filter strips, bio-retention, grass wales, wet and dry, and artificial wetlands [1–3]. The commonly used HDVS is a structural BMP to mitigate anthropogenic and biogenic particulate matter from urban rainfall-runoff into receiving surface waters [4] and has been a favorite choice for profoundly urbanized areas because it can be retrofitted into an existing storm drainage system, thereby decreasing construction costs and requires relatively less space for installation [5]. HDVSs can function as an independent pretreatment facility, and it principally expels particulates and related pollutants using the gravity [6].

Various of HDVSs have been developed to treat urban stormwater overflow and they generally yield faster

* Corresponding author.

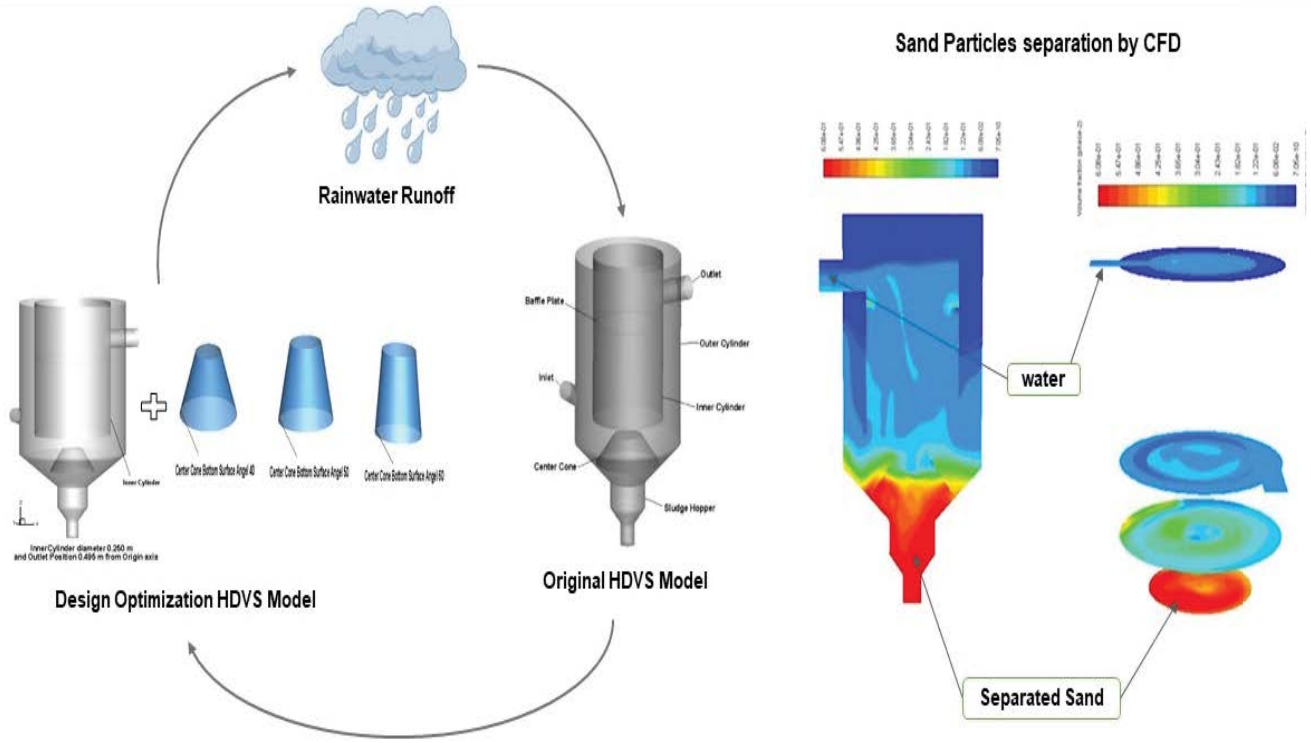

detachment of solids from water in contrast to a conventional settling tank [7]. Rainfall-runoff characteristics and site conditions can differ depending on the performance of HDVSs [8]. Concerning traditional research, computational fluid dynamics (CFD) provides a cost-effective approach to study the flow field of HDVS and lessen risks in equipment modification and process scale-up. A better comprehension of the separation mechanisms of a liquid–solid separator and developed guidelines for HDVS design and operation were validated by CFD simulations [9]. The effects of particle fluid and particle–particle interactions of the stream in a hydro-cyclone and found that the previous interactions played a vital role in the separation productivity [10]. The flocs volume fraction of the outflow and the flow field investigation was performed to analyse the separation performance by increasing hydraulic resident time (HRT) in HDVS [11]. The stream regimes of water and flocs in a HDVS and the impacts of HRT on the flow field and removal efficiency of HDVS [12].

Many prototypes of hydrodynamics separators have been developed for wastewater and stormwater treatment. Additionally, multiple laboratory studies and field tests have been performed. However, with these advances so far, not much fundamental development has been found in the current literature. Structure specifications of commercial separators are derived from empirical equations limited to particular design and specifications of each manufacturer. For a given flow rate and the desired particle removal efficiency, the study endeavors to provide equations that can directly determine of removal efficiency as a function of design flow rate, fluid and solid properties and unit dimensions. The objective of the current study is to theoretically establish some design basis for a selected type of hydrodynamic vortex separator. The aims of current research are as follows:

- Investigation of the velocities flow behavior in hydrodynamics vortex separator through the two-phase flow model.
- Numerically investigate the effects of the inner cylinder diameter and diameter and the position of an outlet on the particle collection performance.
- To determine the optimum center-cone bottom surface cone angle in the HDVS for separation efficiency.
- For optimum inlet position from origin in the HDVS and inlet velocity that has high separation efficiency for sand particle removal.
- Findings that will aid in increasing particle separation performance of hydrodynamic vortex separator.

2. Materials and methods

2.1. Geometric model description

Cyclone equipment applies physical phenomena and gravitates forces to separate material from the fluid. Fig. 1 displays a schematic view that uses inverse flow cyclone and depicts major components and dimensions as mentioned in the reference paper [11]. The particle-laden water introduced from inlet within the hydro cyclone equipment with a larger speed. That completely changes recess configurations such as tangential, radial and axial exist provide larger motility speed. Out of these, the tangential area unit very persistent. The motility flow then falls downward near to the wall through the cyclone body and round shape until a reversal within the axial speed making the water flow move

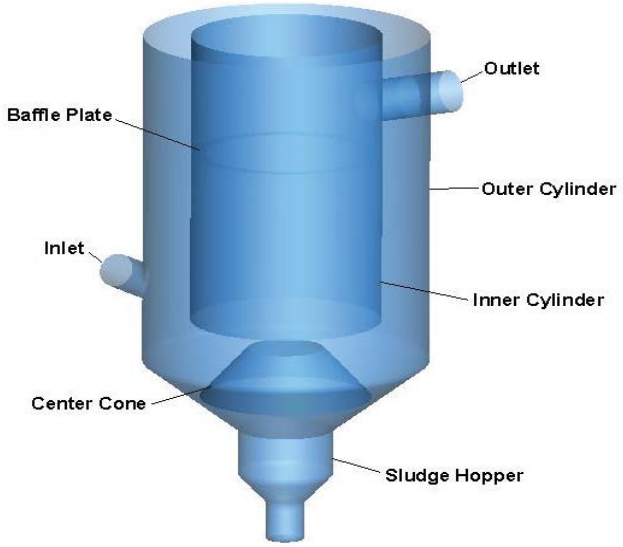

Fig. 1. General structure of the hydrodynamic vortex separator.

in the upwards direction, that happens as a result of the vortex end position.

The solids area unit is separated because of the force and descend helicoidally through the walls of a cyclone and escape the instrumentation across the outlet. The performance of cyclone equipment was measured in the order of the gathering efficiency outlined as a result of the solids fraction separated and in-turn the pressure declined. Naturally, the flow throughout the cyclone equipment is more multiphase (water–solid) and display sturdy water–solid interactions. The water–solid interactions can alone be neglected at a really small solid rate of loadings. Earlier CFD models primarily pay attention to single part flow and turbulence interactions within the cyclone body. CFD simulations of multiphase that were reported for the water–solid interactions and its frequent results relating to cut sizes and grade-efficiency area unit relatively are very limited.

Fig. 1 shows the geometrical model of the hydrodynamic vortex separator that relies on geometrical optimization. The structural dimensions of the model of HDVS employed are illustrated in Table 1. Sand particles are eliminated from water through force and gravity created by the motion of flow within the HDVS by the separation principle.

Parameters setting employed by the reference paper [11] within the HDVS model for calculation of removal potency as shown in Table 2.

2.2. Model development

2.2.1. Major assumptions for sand particle separation

Due to limitation of the computation capability, the flow simulation within the HDVS needs to be simplified to acquire convergence without compromising results accuracy within minimum possible computation time, to achieve the same following assumptions were considered:

- The water continuous section is incompressible and with none air diluted.

Table 1
Geometric dimension for HDVS model from the study by Shi et al. [11]

Structure ID	Diameter/m	Height/m
Outflow pipe	0.05	/
Center height of outflow pipe	/	0.510
Inner cylinder	0.2	0.35
Outer cylinder	0.3	0.4
Cone	Top: 0.3	0.085
	Bottom: 0.1	
Center cone	Top: 0.065	0.06
	Bottom: 0.15	
Inlet pipe	0.04	/
Center height of inlet pipe	/	0.315

Table 2
Simulation parameters from the study by Shi et al. [11]

Property	Value
Water viscosity	0.001 kg^{-1} s^{-1}
Water density	1,000 kg/m^3
Gravitational acceleration	9.8 m/s
Turbulent intensity	5%
Pressure	101, 325 Pa
Restitution coefficient	0.9
Floc diameter	0.06 mm
Floc density	1,060 kg/m^3
Floc viscosity	0.0046 kg^{-1} s^{-1}
Inlet boundary type	Pressure inlet
Outlet boundary type	Pressure outlet
Top surface boundary type	Symmetry

- The influence of inner wall thickness in the cylinder particularly on the flow field is negligible.
- Solid particle area unit is supposed to be elastic and sleek spheres and their volume area unit varies directly to their dry weight. Additionally, no chemical change happens once the particles sediment within the bottom of the sludge hopper [11].

2.2.2. Turbulence model

A strong swirling flow and two-phase separation movement are created by the working process of HDVS, which makes the flow very complex. CFD research on the characteristics of turbulence within a cyclone has recently been conducted. When the flow pattern and particle trajectories are determined in the solid–liquid phase, the Reynolds stress model (RSM), large eddy simulation (LES) model, and k-ε turbulence model tend to be adequate. The computations show that the RSM captures these options, with the isotropic-viscosity k-ε model does not. Specifically, the previous properly represents the physically realistic sensitivity of the flow to disturbances introduced way downstream. However, this terrible

quality makes the process treatment of the flow-exit plane problematic and necessitated the specific prescription of the experimental axial rate across this plane [13].

Several numerical swirl flow measurement methods have been used, including the Standard k-ε turbulent model, the RNG k-ε turbulent model, the RSM and the LES model. In extreme swirling flow, the regular k-ε model and RNG k-ε model had weakness in anisotropic turbulence. The RSM and LES may provide precise predictions of complex turbulence. However, with a highly anisotropic character, RSM may characterize turbulent stress. The RSM prediction was in strong agreement with the experimental results relative to the regular k-ε model and RNG k-ε model. The cyclone separator's internal flow was strong anisotropic turbulence. RSM was extensively shown to be similar to the real anisotropic turbulent flow by abandoning the isotropic eddy-viscosity hypothesis and considering correlation quantities of 2nd orders [14]. Therefore, RSM was used in this study to simulate the solid–liquid phase separation of the HDVS.

2.2.3. Model strategy

Due to the complexity of the flow field, the simulation was categorized into two steps. In the first step, a basic flow field was obtained by using water with a certain density and viscosity. RSM creates the turbulence flow in the model. These distributions in the velocity of the primary phase were further used as an initial part in the secondary phase. In the second step, the multiphase model that is also called the mixture model was turned on. The sand particle was set in the secondary phase with selecting the KTGF model (granular). All simulation parameters employed in the current research are listed in Table 3.

Table 3
Simulation parameters

Properties	Values
Water density	1,000 kg/m^3
Water viscosity	0.001 kg^{-1}s^{-1}
Gravitational acceleration	9.8 m/s
Turbulent intensity	5%
Pressure	101, 325 Pa
Restitution coefficient	0.9
Under-relaxation factor momentum	0.5
Under-relaxation factor kinetic energy	0.5
Under-relaxation factor turbulent dissipation rate	0.5
Inlet velocity	1.44 m/s
Sand particles diameter	0.05, 0.1 and 0.15 mm
Sand particle density	2,650 kg/m^3
Sand particle viscosity	1.7894 e^{-05} kg^{-1} s^{-1}
Inlet boundary type	Pressure inlet
Outlet boundary type	Pressure outlet
Top surface boundary type	Symmetry
Volume fraction	10%

2.2.4. Governing equations

For the HDVS, the two-fluid model needs to be valid. In the TFM model, both primary phase (water) and secondary phase (sand particle) are continuously treated. Conservation of mass and momentum was considered in the mixture model for the both phases. Interface mass transferring was not assumed. The continuity between mixture sections is given within the vector type as below:

$$\frac{\partial}{\partial t}\left(\alpha_m \rho_m\right) + \nabla\left(\alpha_m \rho_m \overrightarrow{v_m}\right) = 0 \tag{1}$$

where α_m is the volume fraction of mixture, t is the time, ρ_m is the density and $\overrightarrow{v_m}$ is the velocity vector.

The momentum balance for the mixture phase is described as follows:

$$\frac{\partial}{\partial t}\left(\rho_m \overrightarrow{v_m}\right) + \nabla\left(\rho_m \overrightarrow{v_m}\overrightarrow{v_m}\right) = \nabla\left[\mu_m\left(\nabla\overrightarrow{v_m} + \nabla\overrightarrow{v_m}^T\right)\right] - \nabla P + \rho_m \vec{g} + \sum \vec{F} + \nabla k_i \rho_i \overrightarrow{v_{d,i}}\overrightarrow{v_{d,i}} \tag{2}$$

where μ_m, P, $\vec{g}$, $\vec{F}$ and $\overrightarrow{v_{d,i}}$, respectively, are the mixture phase viscosity, pressure, acceleration due to gravity, volume force and slip velocity of sand particle.

The conservation of transport and the turbulence viscosity (μ_t) are given below (Fluent User's Guide 2019):

$$\frac{\partial}{\partial t}\left(\rho\overline{v_i' v_j'}\right) + \frac{\partial}{\partial x_k}\left(\rho v_k \overline{v_i' v_j'}\right) = D_{T,ij} + P_{ij} + \varphi_{ij} - \varepsilon_{ij} + F_{ij} \tag{3}$$

$$\mu_t = \rho C_\mu \frac{k^2}{\varepsilon} \tag{4}$$

where the turbulent diffusive transport P_{ij} is the stress production transport, ϕ_{ij} is the pressure strain transport, ε_{ij} is the dissipation. The turbulent viscosity (μ_t) is computed similarly to k-ε model [11].

2.2.5. Particle size distribution

When a stormwater quality equipment is sized, some municipalities ignore a very essential knowledge that encompasses a very significant effect on preventing pollutants from reaching natural waterways particle size distribution (PSD). BMPs area unit usually sometimes sized by their ability to the remove of not defined part of total suspended solids (TSS) defined as a result of the dry mass of solids preserved on a 1-μm filter. Numerous regulation agencies (Various Government Organization) and authorities' unit of area material with just removing 80% of TSS-an accepted traditional for water quality. If a full PSD is not utilized, an inadequate framework might even be implemented, capturing larger coarser particles however, smaller particles pass untreated. Notwithstanding smaller particles are in highest possibility to harm natural water sites. Sediment will be classified into four categories: gravel, sands, silts and clays; their relative size variation can be displayed in Table 4.

Table 4
Display the different particles sizes ranges

Particle	Size range (mm)
Colloids	<0.0001–0.00045
Clay	0.0001–0.002
Silt	0.002–0.05
Sand	0.05–2
Gravel	2–250

Clay and silts have a higher percentage by mass, permitting pollutants (heavy metals, hydrocarbons, nutrients, and so on) to simpler attachment with them. In reality, small size particulates are present up to 80% in the sample's contaminant load, making them the most significant particles for trapping.

2.2.6. Boundary conditions and numerical strategies

The accurate simulation results firmly rely upon the boundary conditions. The HDVS was full of water and still. All velocities and conjointly the amount fraction of water and particles were present there. The precondition for the top surface of the HDVS model was printed as symmetry. Pressure outlet was set at the outlet of the grid surface. Moreover, different surfaces on the grid model were treated as a paper wall. The tangential and axial velocities of the liquid section were set to zero (no-slip condition) at the wall of the cylinder normal speed of the particle was also set at zero. In addition, different water properties, such as density and consistency, were printed as for pure water. For pressure rate coupling semi-implicit methodology pressure connected equation (SIMPLE) was applied. Answer variables of gradients at the cell center by the default setting of least-square cell-based to decrease the machine intensive. For finite-difference pressure, interpolation the pressure staggered selection (PRESTO!) applied that supply a plenty of correct outcomes since interpolation errors and pressure gradients assumptions on boundaries unit avoided. This theme works better for problems with strong body forces (swirl). For the RSM calculation of momentum equations and Reynolds stress to confirm the convergence of the first-order upwind setting. A second-order upwind was utilized for the calculation of turbulent energy and turbulent dissipation rate (Fluent User's Guide, 2019). The condition of convergence for the continuity equation was set at 10^{-6}.

2.2.7. Mesh generation and model validation

2.2.7.1. Grid independence test

On the premise of making a certain accuracy of calculation, it will save calculation by consistent with the affordable range of grids. Studies for grid independence assist to ignore the employment of an associate larger range of cells, whereas final resolution accuracy is constant. The flow field is meshed by the exploitation of the Gambit software system (Version 6.3.2). Simulations were removed at three completely distinctive grids while an increase in grid density to make sure a grid-independent resolution. To inquire about the consequences of CFD results on mesh size, grid refinements with a coarse mesh (500 thousand elements), a fine mesh (1,000 thousand elements), and a finer mesh (2,000 thousand elements) were computed within the simulation method exploitation (Fluent version 2019).

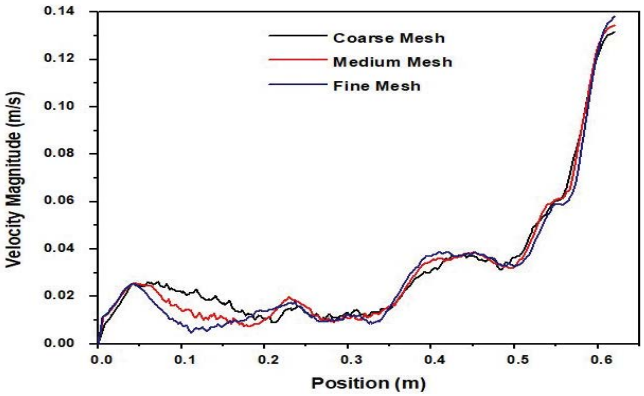

Fig. 2. Velocity magnitude profile with three distinctive mesh sizes.

Fig. 2 displays the results of a simulation for rate magnitude at the center axis of the HDVS for three completely distinctive numbers of the grid nodes. It is seen that for coarse and medium meshes, most of the positions on the line sculpture. The simulated results show the little distinction. However, there is a significant gap between them and therefore the size of fine mesh was considered. The most prominent is that the size of fine mesh. Fine size mesh simulation leads to this section. The trend of the domain rate distribution curve is completely different from that of the previous two size grids.

There are peaks in a very wave crest. At the identical time, the rate distinction between the height and therefore the trough is quite 20%. It is far beyond the allowable range. The distinction decreases with the fineness of the mesh at the identical time, because the range of separate points will increase with the fineness of the mesh, computer computation purpose for calculation the miscalculation is additionally multiplied. The final grid has roughly a 1 million nodes at intervals allowed error vary, a lower mesh size was connected for easy convergence to get an affordable result; however a 3-D CFD simulation with a 1,000 thousand mesh cells was utilized in this research [11].

2.2.7.2. Model validation

Validating of simulation results, the numerical separating potencies were compared with the related experimental results of reference paper [11] and are displayed in Fig. 3. The experimental separation potencies results were gained from the reference paper. It is noted that the removal potency of the experiment compared with simulation reduces along with the drop in the HRT. The simulation results for separation efficiency are in-line with the experiment performed in the reference paper. Nonetheless, the E-E technique with the KTGF model has completely confined the trend of separation potency variates at HRTs and

thus the utility of this method for the development of HDVS geometry and operational condition could not be ignored.

2.2.8. Optimal geometry and operation conditions

For improving the separation productivity of HDVS, the influence of the geometry parameters on the separation efficiency was simulated. The geometric parameters considered in this paper are center cone bottom surface angles, inner cylinder diameter, outlet position and outlet diameter. The geometric parameters not mentioned were taken as the original structure values, the center cone structure exists wide within the style of hydrodynamic vortex separator. The potency of the whirling hydrodynamic vortex separator is one of the key parameters within the style of the design of the hydrodynamic vortex separator. The schematic diagram of the hydrodynamic vortex separator with completely different center cone bottom surface angles, that is, 40, 50 and 60 are shown in Fig. 4.

The schematic diagram of the hydrodynamic vortex separator with different inner cylinder diameter 0.230 m along with outer cylinder 0.330 m and inner cylinder diameter 0.250 m and outer cylinder 0.350 m from origin along with outlet position 0.455 m and 0.495 m is shown in Figs. 5a and b.

The schematic diagram of the hydrodynamic vortex separator with different outlet diameter 0.04 and 0.06 m in Fig. 6a. Diagram with inlet position 0.275 and 0.315 m from origin is shown in Fig. 6b.

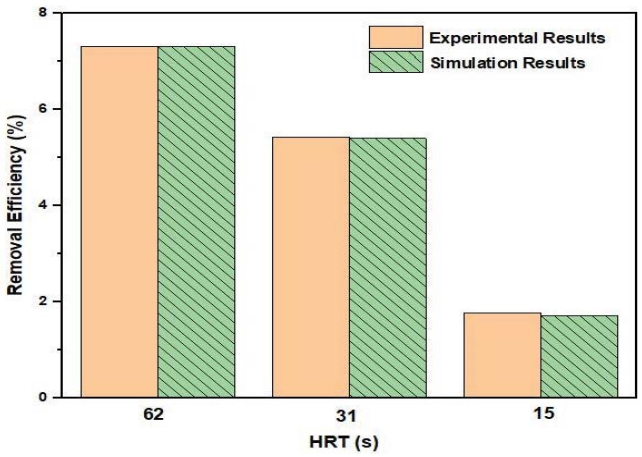

Fig. 3. Removal efficiency comparison at various HRTs.

3. Results

3.1. Effects of center cone bottom surface angles

Effective performance of HDVS relies on a sleek and consistent swirling flow. The study of rate distribution at representative positions of HDVS would facilitate designers to examine its separating potency. For a 3-D downside,

Fig. 4. Three center cone with different bottom surface angles.

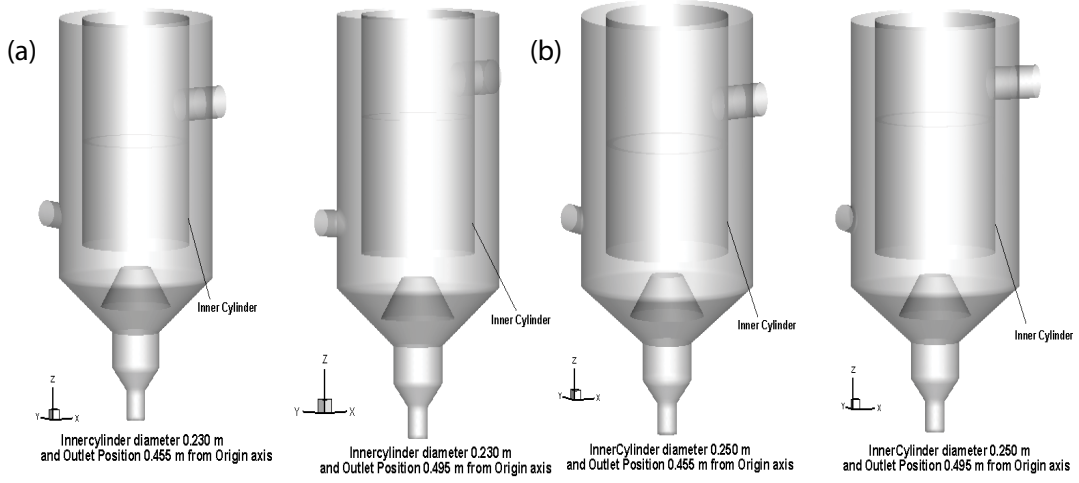

Fig. 5. (a) Structure of HDVS of inner cylinder diameter 0.230 m and outer cylinder 0.330 m and (b) inner cylinder diameter 0.250 m and outer cylinder 0.350 m at the outlet position 0.455 m and 0.495 m from origin.

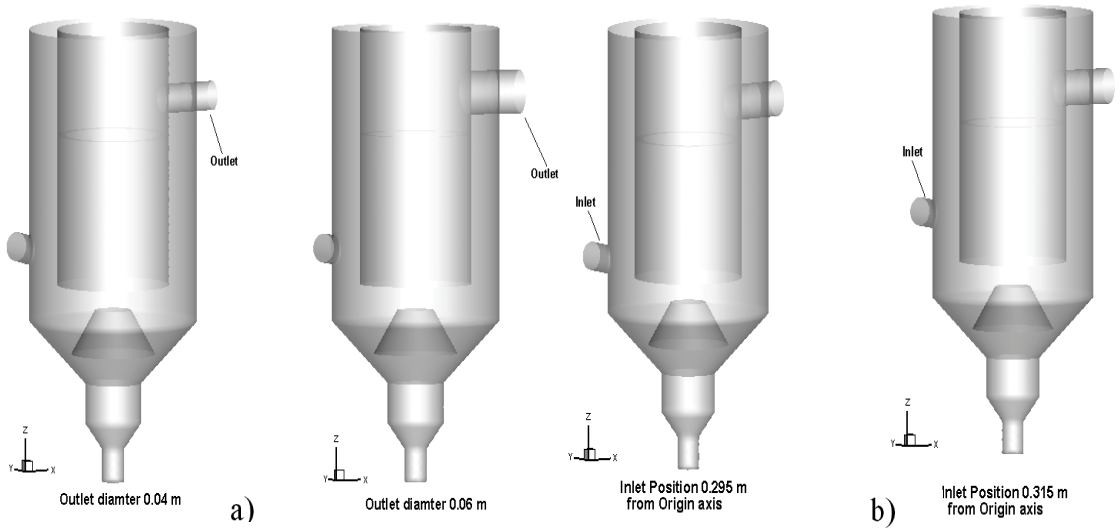

Fig. 6. (a) Structure of the HDVS with different outlet diameter 0.04 m and 0.06 m and (b) with different inlet position diameter 0.275 and 0.315 m from origin.

the speed may be reportable with three components: axial velocity, radial velocity and tangential velocity. Out of them within the swirling flow of an HDVS, the tangential rate is that most significant factor that governs the swirling flow pattern. According to law, an HDVS isolates particles fundamentally by force. The axial flow is vital for transporting particles collected on the walls of the collector. The radial velocity is that the littlest parts and may well be neglected for basic calculations, though it contributes to the transporting particles to the walls.

To demonstrate the flow behavior associate inside an HDVS, the velocity profile on two perpendicular planes at z = 0.315 m and y = 0, covering the method region of the cyclone flow field, are displayed in Fig. 7. It can be seen that velocity magnitude inside the inner flow of the cyclone on the center axis increases from bottom to prime, and additionally, the flow region is split into two areas: quasi-free vortex flow and quasi-forced vortex flow. The elaborated outcomes of those three velocity parts are described as follows.

3.1.1. Tangential velocity

The flow inside a cyclone is usually influenced by the tangential speed and powerful shear among the radial direction that finally ends up, which determines the particle separation. Afterward, long discussion at intervals cyclone centrifuge studies is targeting the tangential speed.

Fig. 8 plots the tangential rate profiles for HDVS with the utterly completely distinctive center cone bottom surface angles on radial line direction. The cyclone has an associate asymmetrical form and conjointly the axis of the cyclone does not exactly coincide with the axis of the vortex. From Fig. 8, it is determined that the water speed is accelerated up and opposite side it reduces once the water spins rotate on the cyclone wall. Flow reversal is taken into account

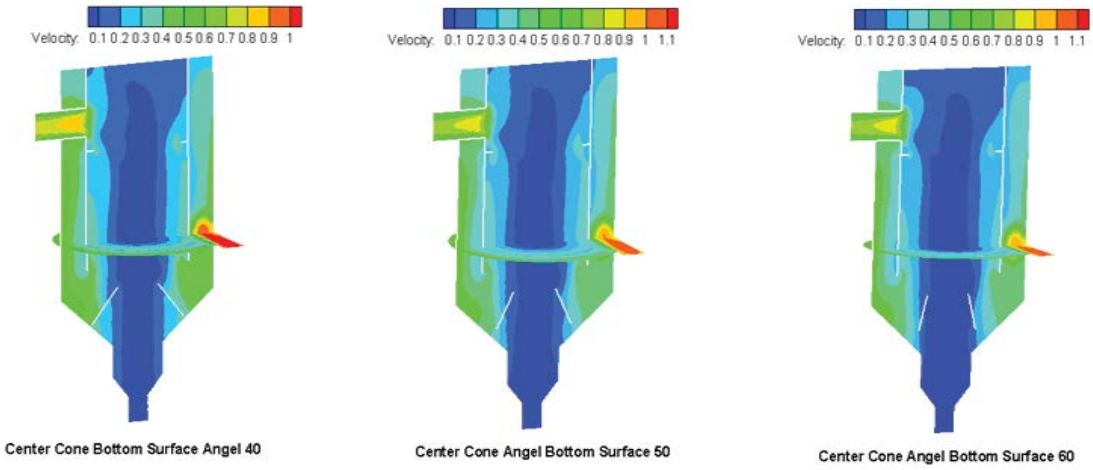

Fig. 7. Velocity magnitude profile representative on two perpendicular planes (x-y at z = 0.315 m and x-z at y = 0) of HDVS with different center-cone bottom surface angles, that is, 40, 50 and 60.

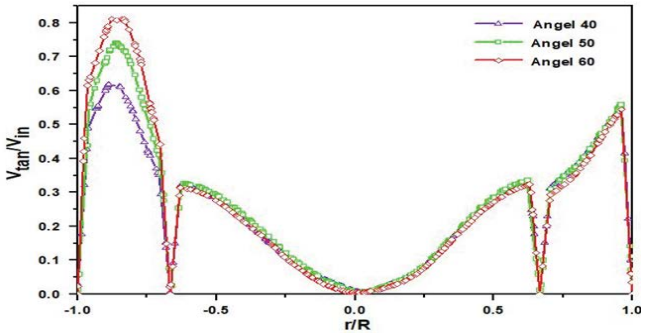

Fig. 8. Tangential velocity profile along radial line in the HDVS with three different center-cone bottom surface angles, that is, 40, 50 and 60.

and conjointly the water flows within the reverse direction to the exit. Once coming back into the inner cylinder, the water collides with the follow-up flow and the rate increases rapidly.

The tangential rate is incredibly dependent on the geometrical design, wall friction and loading of particles. A little reduction is detected at the realm of the inner vortex while increasing the temperature. As a result of the water advancing toward the outlet, the realm of the inner vortex becomes narrower and conjointly the outer vortex becomes wider the foremost reason for the changes in area unit that on increasing the middle cone bottom surface angle. Moreover, the force is directly proportional to the square of the tangential rate, so higher temperature results in the force decreasing so the lower separation intensity.

3.1.2. Axial velocity

The axial velocity of the water part is also having a significant influence on the transportation of particles to the gathering equipment. Empirical models supported the double vortex geometry postulate radially give persistent values for the downward flow within the outer vortex and upward flow among the inner vortex. Each of these values is zero at the axial location where the vortex ended. In reality, the profiles do not appear to be flat but apply maximum and minimum condition. Generally, the descending stream shows surrounding to the walls, whereas the upward flow displays either the most or the lowest at the symmetry axis.

Fig. 9a displays the axial speed profile on the central line. Axial speed is guilty of the two flow streams (downward and upward). It should be seen that, among the out regions, the distribution of speed is almost all positive on the right side and negative at the alternative side. This is often actually because of the vortex rotation regarding the eccentric center due to the non-symmetrical type of the HDVS. However, once a position is negative, three cases all have the descending streams. That refers to water getting in HDVS directly instead of downward direction and reversing to the upward direction, is termed as "lip flow" or "lip leakage".

3.1.3. Radial velocity

The velocity is that the element of sand particles within the direction of radius. In addition, that also contributes to the transporting sand particles to the walls with facilitate of force. Fig. 9b displays velocity plots on the radius of the HDVS with three distinctive center-cone bottom surface angles. Within the left part radial velocity ($r/R < 0$) of radial line, positive value is radially upward, whereas within the right half ($r/R > 0$), those are radially inward. The velocity nearly uniformly distributes in different regions, that accounts the body of water rate has little impact on the dispersion of speed therein the region. The speed affects the particle bypass and may be vital place for confidence in analyzing the particle assortment and losses of efficiency. Frequently the speed is assumed to be smaller magnitude than the other components. However, this can be validated solely within the outer vortex, and particularly close to the vortex finder, the velocity will increase quickly towards the vortex core.

It is seen that there is tiny distinction (small variation) of velocity among three totally different center cone bottom surface angles. The magnitude of the velocity for

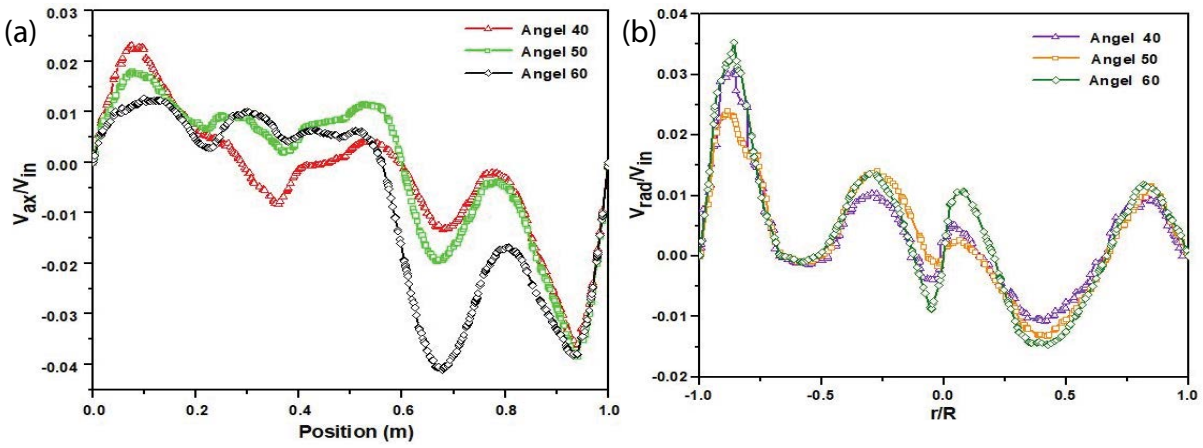

Fig. 9. (a) Axial velocity and (b) radial velocity profile along central line in the HDVS along three different center-cone bottom surface angles, that is, 40, 50 and 60.

center cone bottom surface angle 60 is on top as compared to that of other different angles. High velocity can facilitate the high separation. As a result of the downward particles can expertise (apply) less resistance within the outer spiral flow field within the inner a part of the inner cylinder.

3.1.4. Volume fraction

Fig. 10 shows volume fraction contours on a perpendicular plane (x-z at y = 0) and volume fraction contours on four perpendicular plane (x-y at z = 0.175, 0.235, 0.315 and 0.525 m) in the HDVS along with different center cone bottom surface angles, that is, 40, 50 and 60 for sand particles diameter 0.1 mm and for sand particles diameter 0.05 mm as shown in Figs. 11a and b. The analysis of the sand particle distribution is helpful to determine the performance of HDVS. Generally, center cone bottom surface angle has significant effects on the separation of sand particles. The rise of center cone bottom surface angle increases the flow residence on the sand particle, as well as drag force and pressure gradient force.

Fig. 12a shows the degree fraction plots on the central line of HDVS at totally different bottom surface cone angles for 0.1 mm sand particles diameter. In Fig. 12a it is seen that the volume fraction line is stabilizing for center-cone bottom surface angle 60 as compared with other different center cone bottom surface angles. It is also noted that relative volume fraction is a large value within the sludge hopper, however small at the highest surface. Since the number of sand particles flowing within the HDVS square measure equal, to conclude that reduction in the sand particles separating efficiencies at the totally distinctive center cone bottom surface angles have a discrepancy.

3.1.5. Separation efficiency

The solid volume fraction distribution curve is shown in Fig. 12a with the distinction of diameter, that is, 0.05, 0.1

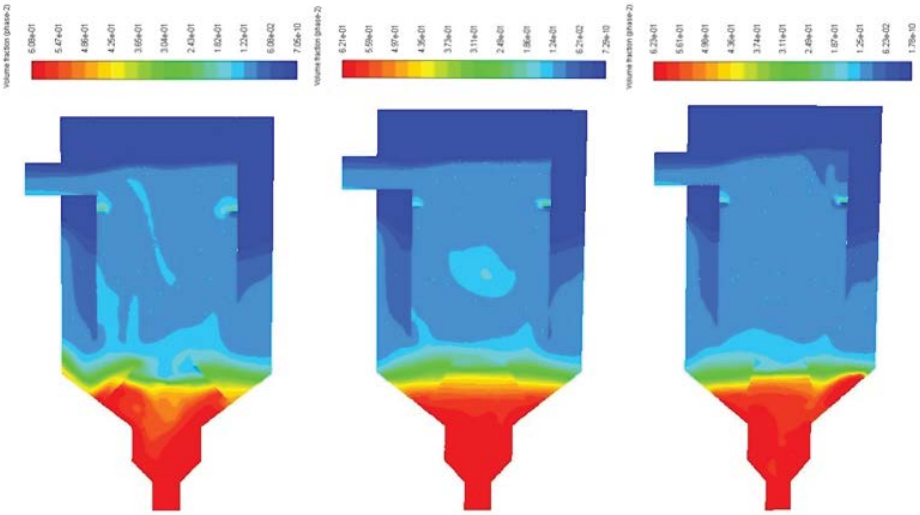

Fig. 10. Volume fraction contours on perpendicular plane (x-z at y = 0) of HDVS along three different center cone bottom surface angles, that is, 40, 50 and 60 for sand particles diameter 0.1 mm.

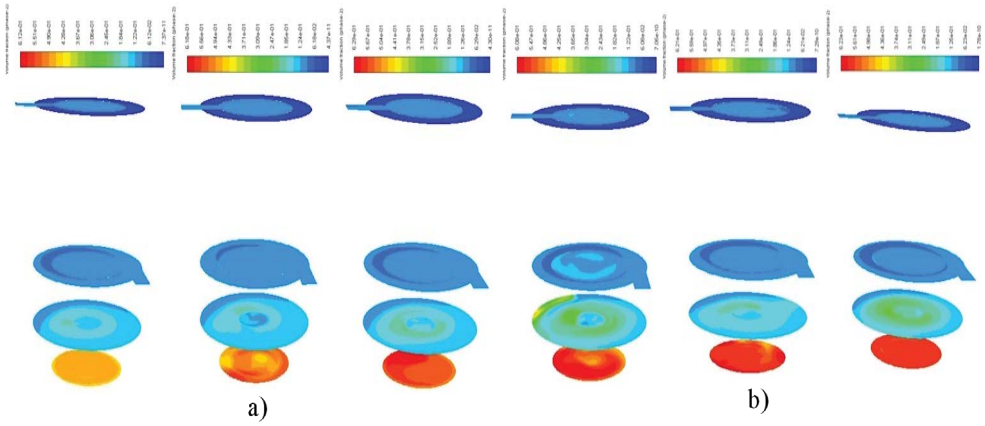

Fig. 11. (a) Volume fraction contours on four perpendicular plane (x-y at z = 0.175, 0.235, 0.315 and 0.525 m) of HDVS along three different center-cone bottom surface angles, that is, 40, 50 and 60 for sand particles diameter 0.1 mm and (b) for sand particles diameter 0.05 mm.

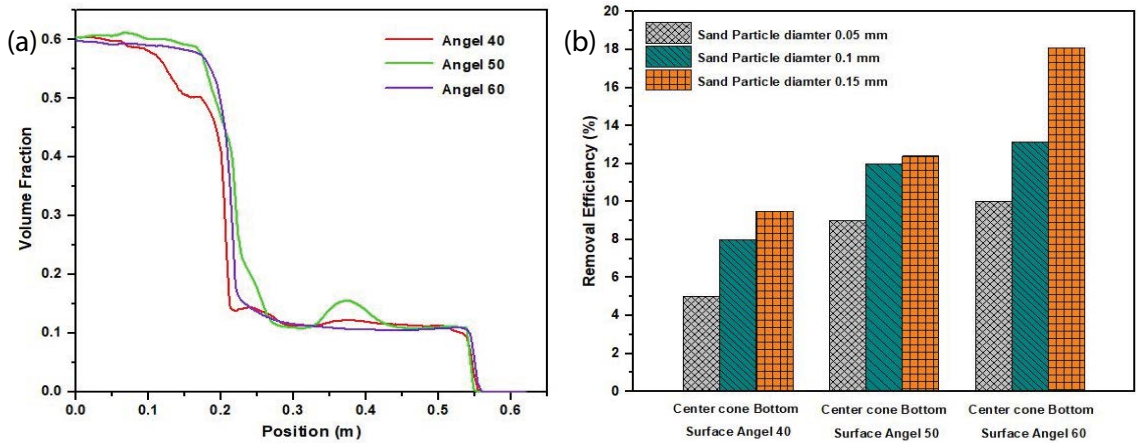

Fig. 12. (a) Volume fraction profile along central line in the HDVS along three different center-cone bottom surface angles 40, 50 and 60 for sand particles diameter 0.1 mm and (b) separation removal efficiency for sand particles diameter 0.05, 0.1 and 0.15 mm.

and 0.15 mm. From this study, we all know that the solid volume fraction of center cone bottom surface cone angle 60 is above those of the center cone bottom surface angles 50 and 40. When center cone bottom surface angle 40, the hydrodynamic vortex separator has reduced separation potency and remains considerably stable. The impact dimension of center cone bottom surface angle 60 has higher separation efficiency. Fig. 12b shows the sand particles removal potency at a diameter of 0.15 mm at center cone bottom surface angle 60, 50 and 40 are 18.1%, 13.5% and 10% respectively. Similarly, for a diameter 0.1 mm center cone bottom surface angle 60 is concerning 12.4%, whereas structure center cone bottom surface 50 and 40 are concerning 12% and 9%. For sand particle diameter 0.05 mm, removal efficiency is 9.5%, 8% and 5%, respectively. Eddy separation potency of the cyclone η is calculated as follows:

$$\eta = \frac{f_{IN} - f_{OF}}{f_{IN}} \times 100\% \quad (5)$$

where f_{IN} is the average value of solid volume fraction at the inlet surface; f_{OF} is the average solid phase volume fraction at the exit surface calculated by the inner cylinder hydrodynamic vortex separator.

3.2. Effects of inner cylinder diameter 0.250 m

3.2.1. Volume fraction

Fig. 13 shows volume fraction contours of four perpendicular planes (*x-y* at *z* = 0.175, 0.235, 0.315 and 0.525 m) in the HDVS for the inner cylinder diameter 0.250 m and outlet position 0.495 m for sand particles diameter 0.05, 0.1 and 0.15 mm, respectively.

Fig. 14 shows volume fraction contours on four perpendicular planes (*x-y* at *z* = 0.175, 0.235, 0.315 and 0.480 m) in the HDVS along inner cylinder diameter 0.250 m and outlet position 0.455 m for sand particles diameter 0.05, 0.1 and 0.15 mm. Generally, inner cylinder diameter 0.250 m along outlet position 0.495 m has significant effects on the separation of sand particles. The rise (increase) of outlet position can increase force which gains the flow residence time on the sand particles, as well as drag and pressure gradient force.

3.2.2. Separation efficiency

Fig. 15 shows the sand particles removal potency at a diameter of 0.15 mm for inner cylinder diameter 0.250 m and outlet positions 0.495 and 0.455 m, the efficiency is 12% and 8%, respectively. Similarly, for diameter 0.1 mm, inner

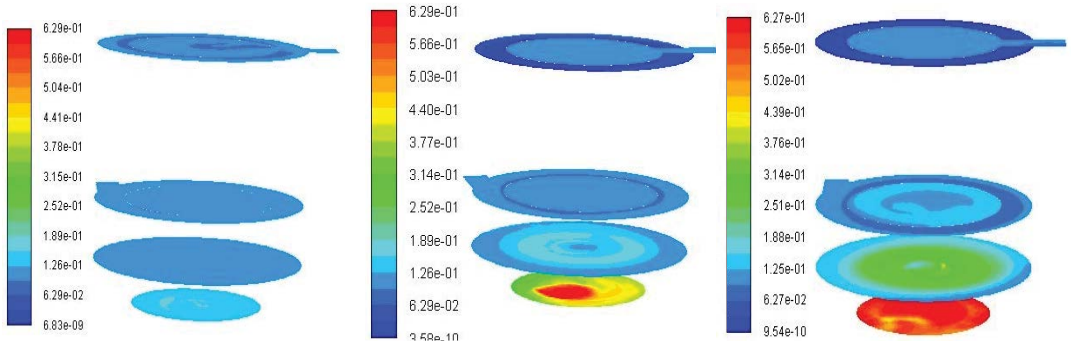

Fig. 13. Volume fraction contours on four perpendicular plane (*x-y* at *z* = 0.175, 0.235, 0.315 and 0.525 m) in the HDVS with inner cylinder diameter 0.250 m and outlet position 0.495 m for sand particle diameter 0.05, 0.1 and 0.15 mm.

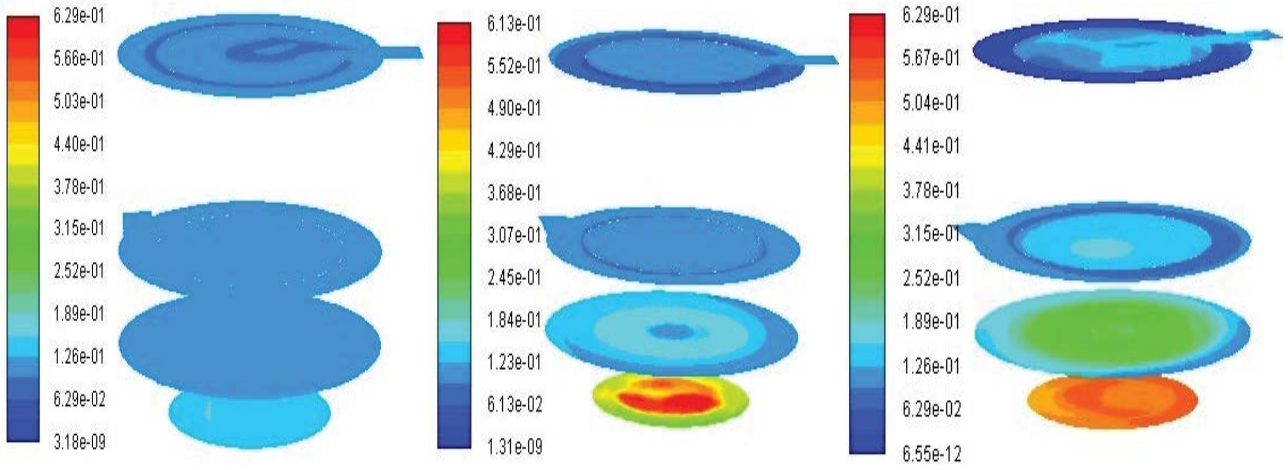

Fig. 14. Volume fraction contours on four perpendicular plane (*x-y* at *z* = 0.175, 0.235, 0.315 and 0.480 m) in the HDVS with inner cylinder diameter 0.250 m and outlet position 0.455 m for sand particle diameter 0.05, 0.1 and 0.15 mm.

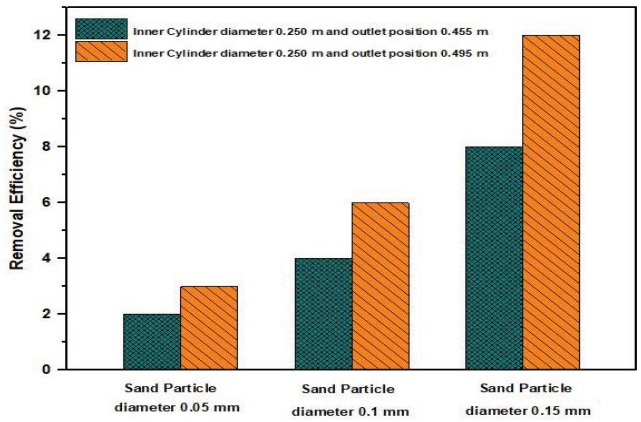

Fig. 15. Separation removal efficiency in the HDVS with inner cylinder diameter 0.250 m and outlet position 0.455 and 0.495 m for sand particle diameter 0.05, 0.1 and 0.15 mm.

cylinder diameter 0.250 m and outlet positions 0.495 m concerning 6%, whereas outlet position 0.455 m concerning 4%. For sand particle diameter 0.05 mm at outlet position 0.495 and 0.455 m, the removal efficiency is 3% and 2%, respectively.

3.3. Effects of inner cylinder diameter 0.230 m

3.3.1. Volume fraction

Fig. 16 shows the volume fraction contours on four perpendicular planes (*x-y* at *z* = 0.175, 0.235, 0.315 and 0.525 m) in the HDVS along inner cylinder diameter 0.230 m and outlet position 0.495 m for sand particles diameter 0.05, 0.1 and 0.15 mm.

Fig. 17 shows the volume fraction contours on four perpendicular planes (*x-y* at *z* = 0.175, 0.235, 0.315 and 0.480 m) in the HDVS along inner cylinder diameter 0.230 m and outlet position 0.455 m for sand particles diameter 0.05, 0.1 and 0.15 mm. Generally, inner cylinder diameter 0.230 m along with outlet position 0.495 m has significant effects on the separation of sand particles. The rise of outlet position increase force which will gain the flow residence time on the sand particle, as well as drag and pressure gradient force.

3.3.2. Separation efficiency

Fig. 18 shows the sand particles removal potency at a diameter of 0.15 mm for inner cylinder diameter 0.230 m and outlet positions 0.495 and 0.455 m efficiency is 9% and 7% respectively. Similarly, for a diameter 0.1 mm for inner cylinder diameter 0.230 m and outlet positions 0.495 m concerning 6%, whereas outlet position 0.455 m concerning 4.2%. For sand particle diameter 0.05 mm at outlet position 0.495 and 0.455 m removal efficiency is 3.3% and 2%, respectively.

3.4. Effects of inlet position

3.4.1. Volume fraction

Fig. 19 shows the volume fraction contours on four perpendicular plane (*x-y* at *z* = 0.175, 0.235, 0.335 and 0.510 m) in the HDVS along inlet position 0.315 m from origin for sand particles diameter 0.05, 0.1 and 0.15 mm.

Fig. 20 shows the volume fraction contours on four perpendicular plane (*x-y* at *z* = 0.175, 0.235, 0.335 and 0.510 m) in the HDVS along inlet position 0.275 m for sand particles diameter 0.05, 0.1 and 0.15 mm. Generally, inlet position 0.315 m has significant effects on the separation of sand particles. The rise of outlet diameter can increase force and gain the flow residence on the sand particles, as well as drag force and pressure gradient force.

3.4.2. Separation efficiency

Fig. 21 shows the sand particles removal potency at a diameter of 0.15 mm for inlet position 0.315 m and 0.275 m efficiency is 8% and 6% respectively. Similarly, for a diameter 0.1 mm for inlet position 0.315 m concerning 5%, whereas and 0.275 m concerning 4%. For sand particle diameter

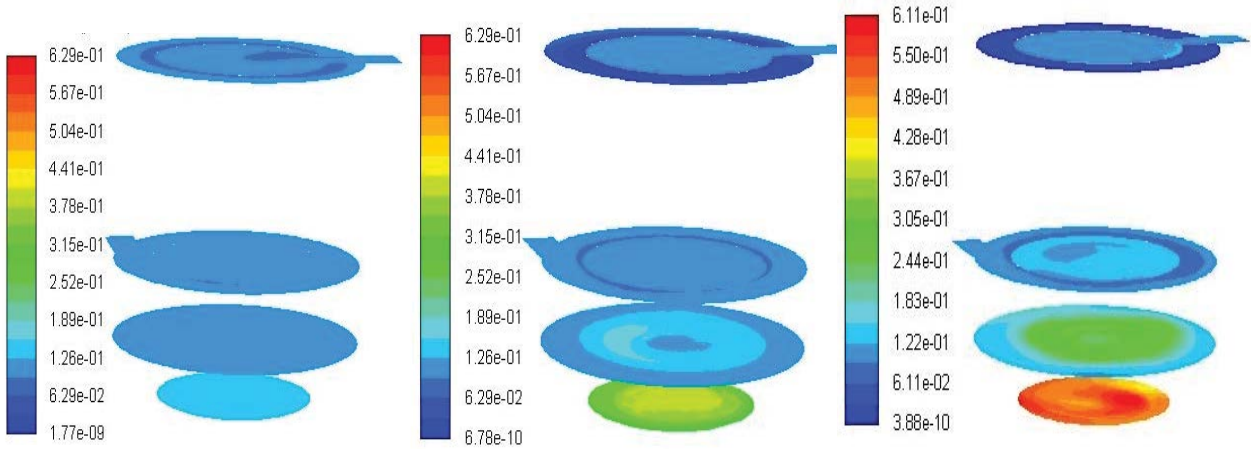

Fig. 16. Volume fraction contours on four perpendicular plane (*x-y* at *z* = 0.175, 0.235, 0.315 and 0.495 m) in the HDVS with inner cylinder diameter 0.230 m and outlet position 0.495 m for sand particle diameter 0.05, 0.1 and 0.15 mm.

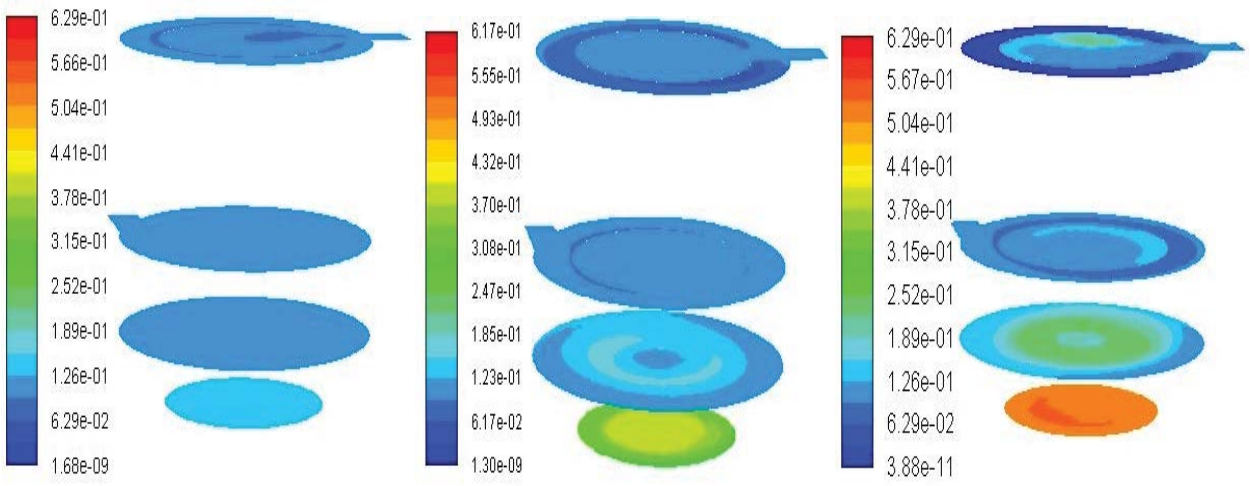

Fig. 17. Volume fraction contours on four perpendicular plane (*x-y* at *z* = 0.175, 0.235, 0.315 and 0.480 m) in the HDVS with inner cylinder diameter 0.230 m and outlet position 0.455 m for sand particle diameter 0.05, 0.1 and 0.15 mm.

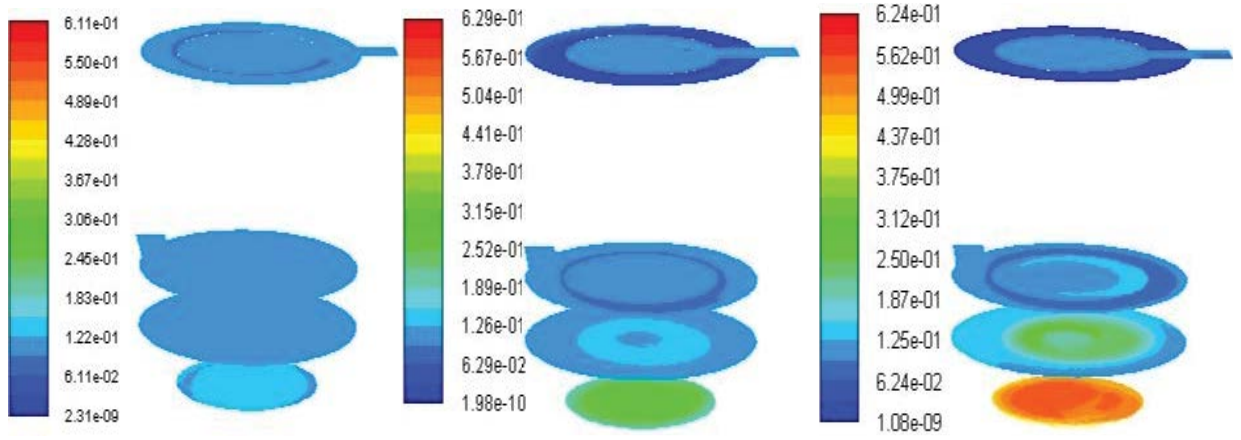

Fig. 18. Separation removal efficiency in the HDVS with inner cylinder diameter 0.230 m and outlet position 0.455 and 0.495 m for sand particle diameter 0.05, 0.1 and 0.15 mm.

0.05 mm at inlet position 0.315 m and 0.275 m removal efficiency is 3% and 1.7%, respectively.

3.5. Effects of inlet velocity

3.5.1. Volume fraction

Fig. 22 volume fraction contours on four perpendicular planes (*x-y* at *z* = 0.175, 0.235, 0.335 and 0.510 m) in the HDVS along inlet velocity 0.36 m/s for sand particles diameter 0.05, 0.1 and 0.15 mm.

Fig. 23 shows the volume fraction contours on four perpendicular planes (*x-y* at *z* = 0.175, 0.235, 0.335 and 0.510 m) in the HDVS along inlet velocity 0.72 m/s for sand particles diameter 0.05, 0.1 and 0.15 mm. Generally, inlet velocity 0.36 m/s has significant effects on the separation of sand particles.

3.5.2. Separation efficiency

Fig. 24 shows the sand particles removal potency at diameter of 0.15 mm for inlet velocities 0.36 and 0.72 m/s efficiencies are 40% and 18% respectively. Similarly, for diameter 0.1 mm for inlet position 0.36 m/s concerning 20%, whereas and 0.72 m/s concerning 11%. For sand diameter 0.05 mm at inlet velocities 0.36 and 0.72 m/s, removal efficiencies are 5% and 3%, respectively.

3.6. Effects of outlet diameter

3.6.1. Volume fraction

Fig. 25 shows the volume fraction contours on four perpendicular plane (*x-y* at *z* = 0.175, 0.235, 0.315 and 0.530 m) in the HDVS along outlet diameter 0.06 m for sand particles diameter 0.05, 0.1 and 0.15 mm.

Fig. 26 shows the volume fraction contours on four perpendicular plane (*x-y* at *z* = 0.175, 0.235, 0.315 and 0.520 m) in the HDVS along outlet diameter 0.04 m for sand particles diameter 0.05, 0.1 and 0.15 mm. Generally, outlet diameter of 0.06 m has significant effects on the separation of sand particles. The rise of outlet diameter can increase force it will gain the flow residence on the sand particles, as well as drag force and pressure gradient force.

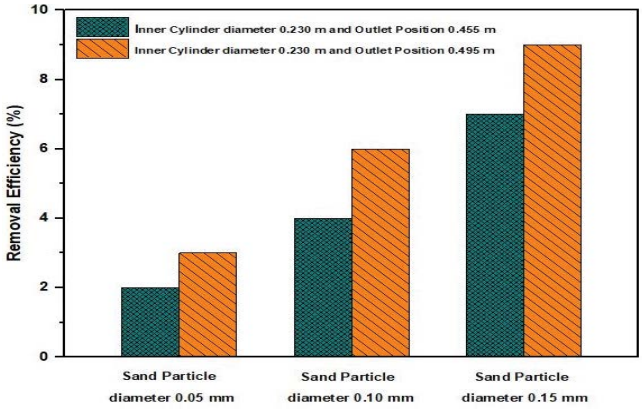

Fig. 19. Volume fraction contours on four perpendicular planes (*x-y* at *z* = 0.175, 0.235, 0.295 and 0.510 m) in the HDVS inlet position 0.315 m from origin for sand particle diameter 0.05, 0.1 and 0.15 mm.

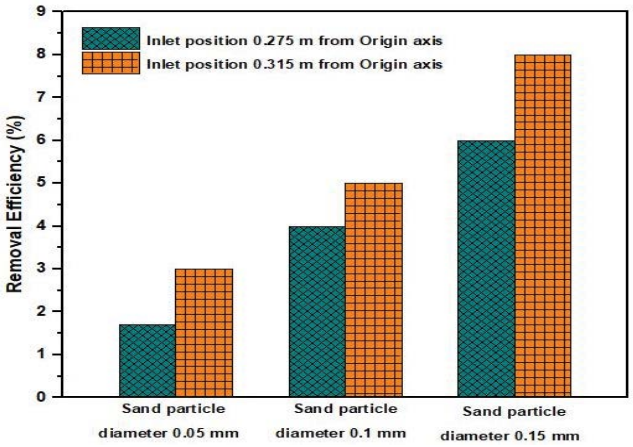

Fig. 21. Separation removal efficiency with inlet position 0.275 m and 0.335 m for sand particle diameter 0.05, 0.1 and 0.15 mm.

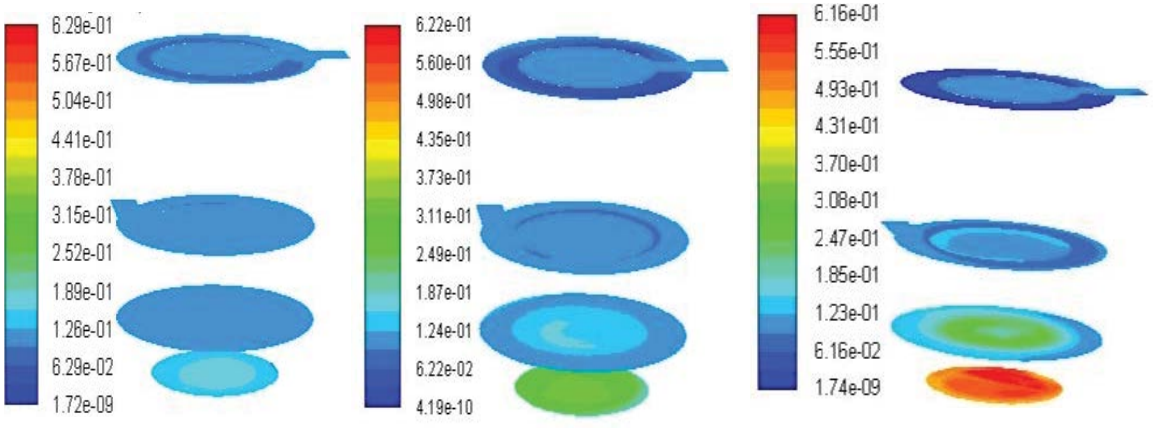

Fig. 20. Volume fraction contours on four perpendicular plane (*x-y* at *z* = 0.175, 0.235, 0.295 and 0.510 m) in the HDVS with inlet 0.275 m for sand particle diameter 0.05, 0.1 and 0.15 mm.

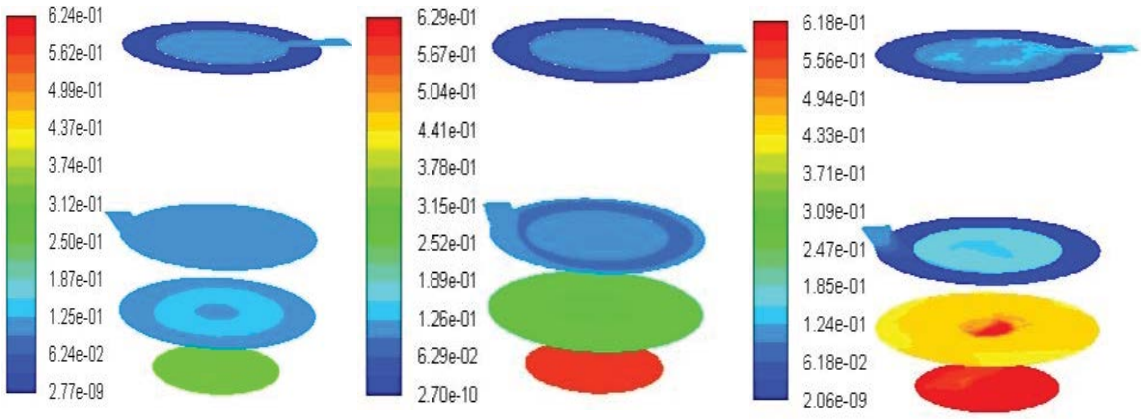

Fig. 22. Volume fraction contours on four perpendicular plane (*x-y* at *z* = 0.175, 0.235, 0.315 and 0.510 m) in the HDVS inlet velocity 0.36 m/s for sand particle diameter 0.05, 0.1 and 0.15 mm.

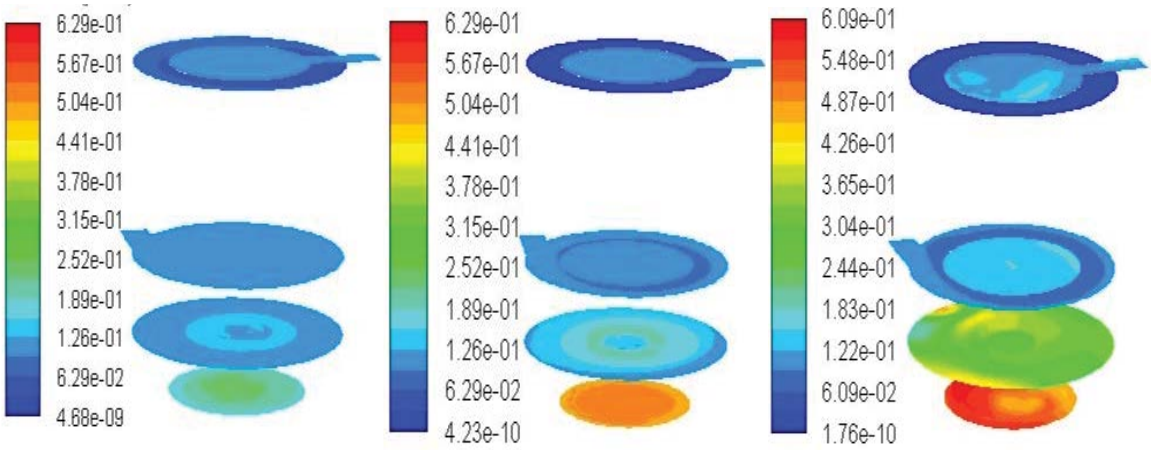

Fig. 23. Volume fraction contours on four perpendicular planes (*x-y* at *z* = 0.175, 0.235, 0.315 and 0.510 m) in the HDVS with inlet 0.275 m for sand particle diameter 0.05, 0.1 and 0.15 mm.

3.6.2. Separation efficiency

Fig. 27 shows the sand particles removal potency at a diameter of 0.15 mm for outlet diameter 0.06 and 0.04 m efficiency is 9% and 7% respectively. Similarly, for a diameter 0.1 mm for inner cylinder diameter 0.230 m and an outlet diameter of 0.06 m concerning 4%, whereas outlet diameter 0.04 m concerning 3%. For sand particle diameter 0.05 mm at outlet diameter 0.06 and 0.04 m removal efficiency is 2% and 1.7%, respectively.

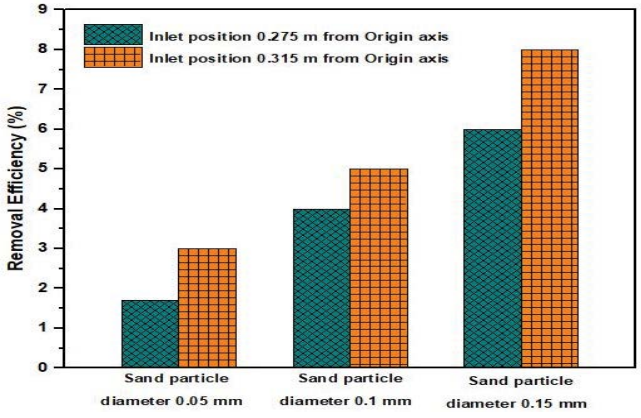

Fig. 24. Separation removal efficiency with inlet velocities 0.36 and 0.72 m/s for sand particle diameter 0.05, 0.1 and 0.15 mm.

4. Discussion

For verification purposes, a comparative procedure was carried out. Comparison of the acquired results through the use of research approaches, with the experimental results was taken from the previous studies. The validation carried out was aimed at the quantitative estimation of the errors resulting from the numerical model assumptions and the parametrization of the approximation and boundary conditions. The application of a counter-cone in each of the studied geometrical variants leads to an increase in solid particle separation [15]. The elongation of the cylindrical part improves the particle separation performance in this hydro cyclone [16]. The numerical simulation of the flow field distribution in the cyclone separator by CFD was important for understanding its working theory, separation characteristics

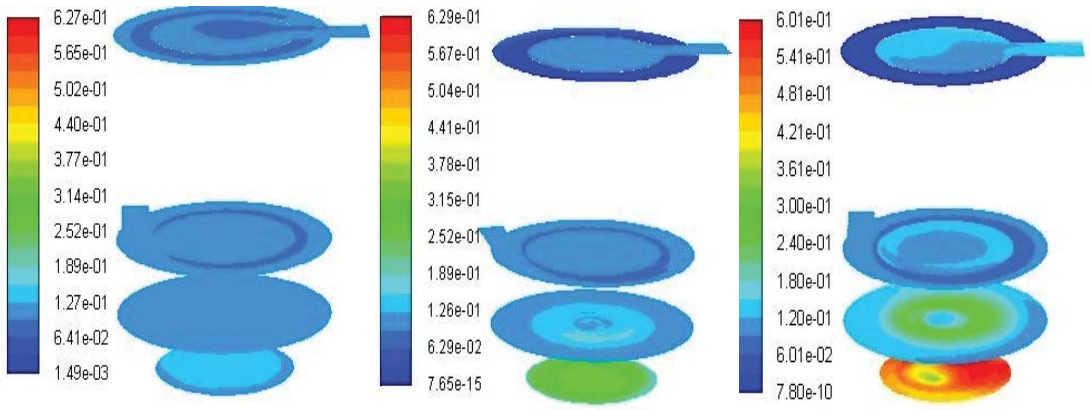

Fig. 25. Volume fraction contours on four perpendicular plane (*x-y* at *z* = 0.175, 0.235, 0.315 and 0.530 m) in the HDVS outlet diameter 0.06 m for sand particle diameter 0.05, 0.1 and 0.15 mm.

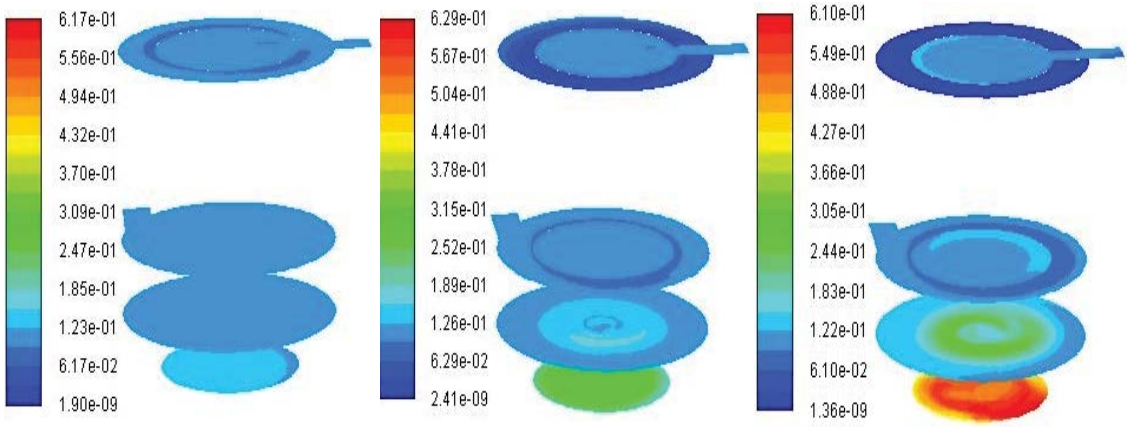

Fig. 26. Volume fraction contours on four perpendicular plane (*x-y* at *z* = 0.175, 0.235, 0.315 and 0.520 m) in the HDVS with outlet diameter 0.04 m for sand particle diameter 0.05, 0.1 and 0.15 mm.

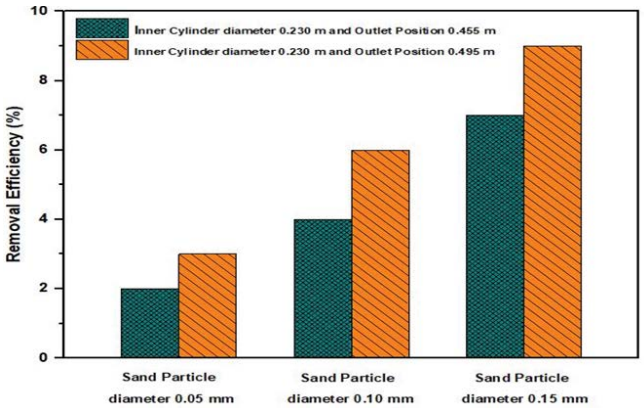

Fig. 27. Separation removal efficiency with outlet diameter 0.04 and 0.06 m for sand particle diameter 0.05, 0.1 and 0.15 mm.

and structural optimization design. This study examined the impact on the particle separation rate of six different structural parameters so that the particle separation rate is more than 95% for particles larger than 10 μm in diameter [14]. Imperfections in the calculation models that involve the implementation of certain simplifications and empirical coefficients with high levels of uncertainty result in slight differences. The basic indicators used to test the proposed modifications and their effect on cyclone separator efficiency were obtained. The difference between the results of numerical simulation and those of experiment in the separation efficiency of the introduced geometry modifications hopefully to be small because the original numerical model has been checked the experiment of other researchers in the subsection of 2.7.2.

5. Conclusion

In the current research, the flow data of HDVS used for stormwater runoff system at HDVS with different center-cone bottom surface angles, increase of inner cylinder diameter with different outlet position from origin and outlet diameter supported the CFD code. In the current research, the flow data of HDVS used for stormwater runoff system at HDVS with different center-cone bottom surface angles, the increase of inner cylinder diameter with different outlet position from origin and outlet diameter in order to enhance the separation potency of HDVS for storm runoff to get rid of sand particles. Moreover,

the tangential, axial and velocity profile and volume fraction distribution of sand particles with different diameters (i.e., 0.05, 0.1 and 0.15 mm) inside the HDVS area unit were investigated. The simulation of solid–liquid part flow within the HDVSs was conducted on RSM and Eulerian–Eulerian multiphase 3-D model combined with the kinetic theory of granular flow, which specially analyzed the rate contours, recess and outlet volume fraction of solid phase.

The simulation results showed that with an increase of center-cone bottom surface angle, increase of inner cylinder diameter and outlet position from origin the velocity and also increase of outlet diameter field below the inlet part and surrounding part of the inner cylinder had small difference at an inlet velocity of 1.44 m/s. However, the distinction of results of an inner region of the inner cylinder was stark and therefore the turbulence was increased during this region. Some swirls occurred within the inner zone of the inner cylinder that another energy waste and had a negative impact on the sand particles separation. The separation efficiency of HDVS had a positive relationship with the increase of center-cone bottom surface angle, increase of inner cylinder diameter along with outlet position from origin and increase the outlet diameter.

- Sand particles removal potency at a diameter of 0.15 mm at center cone bottom surface angle 60, 50 and 40 is 18.1%, 13.5% and 10% respectively. Similarly, for a diameter 0.1 mm center cone bottom surface angle 60 is concerning 12.4%, whereas structure center cone bottom surface 50 and 40 are concerning 12% and 9%. For sand particle diameter 0.05 mm removal efficiency is 9.5%, 8% and 5%, respectively.
- Sand particles removal potency at a diameter of 0.15 mm for inner cylinder diameter 0.250 m and outlet positions 0.495 m and 0.455 m efficiency is 12% and 8% respectively. Similarly, for a diameter 0.1 mm for inner cylinder diameter 0.250 m and outlet positions 0.495 m concerning 6%, whereas outlet position 0.455 m concerning 4%. For sand particle diameter 0.05 mm at outlet position 0.495 and 0.455 m removal efficiency is 3% and 2%, respectively.
- Sand particles removal potency at a diameter of 0.15 mm for inner cylinder diameter 0.230 m and outlet positions 0.495 and 0.455 m efficiency is 9% and 7% respectively. Similarly, for a diameter 0.1 mm for inner cylinder diameter 0.230 m and outlet positions 0.495 m concerning 6%, whereas outlet position 0.455 m concerning 4.2%. For sand particle diameter 0.05 mm at outlet position 0.495 and 0.455 m removal efficiency is 3.3% and 2%, respectively.
- Sand particles removal potency at a diameter of 0.15 mm for inlet position 0.315 and 0.275 m efficiency is 8% and 6% respectively. Similarly, for a diameter 0.1 mm for inlet position 0.315 m concerning 5%, whereas and 0.275 m concerning 4%. For sand particle diameter 0.05 mm at inlet position 0.315 and 0.275 m removal efficiency is 3% and 1.7%, respectively.
- Sand particles removal potency at diameter of 0.15 mm for inlet velocities 0.36 and 0.72 m/s efficiencies are 40% and 18% respectively. Similarly, for diameter 0.1 mm for inlet position 0.36 m/s concerning 20%, whereas and 0.72 m/s concerning 11%. For sand particle diameter 0.05 mm at inlet position 0.36 and 0.72 m/s removal efficiencies are 5% and 3%. respectively.
- Sand particles removal potency at a diameter of 0.15 mm for outlet diameter 0.06 and 0.04 m efficiency is 9% and 7% respectively. Similarly, for diameter 0.1 mm for the inner cylinder diameter 0.230 m and outlet diameter 0.06 m concerning 4%, whereas outlet diameter 0.04 m concerning 3%. For sand particle diameter 0.05 mm at outlet diameter 0.06 and 0.04 m removal efficiency is 2% and 1.7%, respectively.

For further study, the mathematical model established in this paper still has some assumptions, such as simplification of various shapes, size of particles and granules (granular characteristics, stress, etc.) and hypothesis of TSS in rain runoff. To research the influence of various particles on the flow field, the simulation will be used. On the idea of the prevailing simulation results, the pilot-scale hydrodynamic vortex separator for rainfall-runoff system analysis is concentrated. Interesting and new conclusions are used to increase particle separation performance within the hydrodynamic vortex separator.

Acknowledgments

This work was supported by the Tianjin technical innovation guidance project program (16YDLJSF00030) and the key projects in the control and management of national polluted water bodies (2017ZX07106001).

References

[1] A.P. Davis, Field performance of bio-retention: water quality, Environ. Eng. Sci., 24 (2007) 1048–1064.
[2] K. Lee, H. Kim, G. Pak, S. Jang, L. Kim, C. Yoo, Z. Yun, J. Yoon, Cost-effectiveness analysis of stormwater best management practices (BMPs) in urban watersheds, Desal. Water Treat., 19 (2010) 92–96.
[3] J.R. Vogel, T.L. Moore, R.R. Coffman, S.N. Rodie, S.L. Hutchinson, K.R. McDonough, A.J. McLemore, J.T. McMaine, Critical review of technical questions facing low impact development and green infrastructure: a perspective from great plains, Water Environ. Res., 87 (2015) 849–862.
[4] J.J. Sansalone, S.S. Pathapati, Particle dynamics in a hydrodynamic separator subject to transient rainfall-runoff, Water Resources Res., 45 (W09408) (2009) 1–14.
[5] D. Saddoris, O Mohseni, J. Gulliver, Assessing Hydrodynamic Separator Under High water Flow Condition, World Environmental & Water Resources Congress, 2009, pp. 864–874.
[6] M.A. Wilson, O. Mohseni, J.S. Gulliver, R.M. Hozalski, H.G. Stefan, Assessment of hydrodynamic separators for storm-water treatment, J. Hydraul. Eng., 135 (2009) 383–392.
[7] K.H. Kwon, S.W. Kim, L.H. Kim, J.H. Kim, S. Lee, K.S. Min, Particle removal properties of stormwater runoff with lab-scale vortex separator, Desal. Water Treat., 38 (2012) 349–353.
[8] D. Tran, J.H. Kang, Optimal design of a hydrodynamic separator for treating runoff from roadways, J. Environ. Manage., 116 (2013) 1–9.
[9] J.P. Veerapen, B.J. Lowry, M.F. Couturier, Design methodology for the swirl separator, Aquacult. Eng., 33 (2005) 21–45.
[10] W. Kraipech, A. Nowakowski, T. Dyakowski, A. Suksangpanomrung, An investigation of the effect of the particle-fluid and particle-particle interactions on the flow within a hydrocyclone, Chem. Eng. J., 111 (2005) 189–197.
[11] M.M. Shi, Y.J. Ruan, J.P. Li, Z.Y. Ye, G. Liu, S.M. Zhu, Numerical study of dense solid-liquid flow in hydrodynamic vortex

separator applied in recirculating bio-floc technology system, Aquacult. Eng., 79 (2017) 24–34.
[12] M. Shi, Y. Ruan, B. Wu, Z. Ye, S. Zhu, Performance Evaluation of hydrodynamic vortex separator at different hydraulic retention times applied in recirculating biofloc technology system, J. ASABE, 60 (2017) 1737–1747.
[13] S. Hogg, M.A. Leschziner, Computation of highly swirling confined flow with a Reynolds stress turbulence model, AIAA J., 27 (1989) 57–63.
[14] Y. Yuan, Z. Zhao, L. Tan, Y. Xu, Y. Yuan, Structural improvement of the cyclone separator for separating the biogas impurity particles, Energy Sour. Part A, (2020). https://doi.org/10.1080/15567036.2020.1815905
[15] M. Wasilewski, Analysis of the effect of counter-cone location on cyclone separator efficiency, Sep. Purif. Technol., 179 (2017) 236–247.
[16] Q. Zhou, Ch. Wang, H. Wang, J. Wang, Eulerian–Lagrangian study of dense liquid-solid flow in an industrial-scale cylindrical hydro cyclone, Int. J. Mineral Process., 151 (2016) 40–50.